

## Spin and valley polarization dependence of resistivity in two dimensions

K. Takashina,<sup>1</sup> Y. Niida,<sup>1,2</sup> V. T. Renard,<sup>3</sup> B. A. Piot,<sup>4</sup> D. S. D. Tregurtha,<sup>1</sup> A. Fujiwara,<sup>5</sup> and Y. Hirayama<sup>2</sup>

<sup>1</sup>*Department of Physics, University of Bath, Bath BA2 7AY, United Kingdom*

<sup>2</sup>*Graduate School of Science, Tohoku University, 6-3 Aramaki-za Aoba, Aobaku, Sendai, 980-8578 Japan*

<sup>3</sup>*SPSMS, UMR-E 9001, CEA-INAC/UJF-Grenoble 1, Grenoble F-38054, France*

<sup>4</sup>*Laboratoire National des Champs Magnétiques Intenses, CNRS-UJF-UPS-INSA, 38042 Grenoble, France*

<sup>5</sup>*NTT Basic Research Laboratories, NTT Corporation, Atsugi-shi, Kanagawa 243-0198, Japan*

(Received 24 May 2013; published 4 November 2013)

We demonstrate that spin polarization and valley polarization have quantitatively similar effects on the resistivity of a two-dimensional electron gas in a silicon-on-insulator quantum well. In so doing, we also examine the dependence on disorder, leading to a coarse but global phenomenology of how the resistivity depends on its key parameters: spin and valley polarization, density, disorder, and temperature.

DOI: [10.1103/PhysRevB.88.201301](https://doi.org/10.1103/PhysRevB.88.201301)

PACS number(s): 73.40.Qv, 71.30.+h, 75.47.-m

In addition to the spin degree of freedom which is widely known to be pivotal in determining the resistivity of two-dimensional electronic systems (2DES),<sup>1-4</sup> charge carriers in a number of important and topical materials such as silicon, diamond, graphene, MoS<sub>2</sub>, and aluminium arsenide possess a valley degree of freedom due to band degeneracy. Science and technology exploiting this degree of freedom, now often referred to as valleytronics, is a subject of surging interest.<sup>5</sup> However, unlike spin, which usually couples strongly to an external magnetic field, techniques for controlling valley splitting and valley polarization are more material specific, raising challenges for exploring its impact on resistivity.

Experiments probing the physics of valley polarization in steady-state transport have been largely limited to the forerunning work on AlAs,<sup>6</sup> in which valley polarization is achieved by applying symmetry-breaking strain. These have revealed remarkable valley-dependent phenomena such as in the behavior of fractional quantum Hall states<sup>7</sup> and impressive similarities between spin and valley, for example, in the behavior of valley susceptibility<sup>8</sup> and the qualitative role played by valleys in the apparent metal-insulator transition.<sup>9</sup> However, these experiments are complicated by the in-plane anisotropy of effective mass, and the extent to which the results are general and applicable to silicon, the archetypical semiconductor in which most studies of the metal-insulator transition have been undertaken<sup>1-3</sup> and which continues to reveal new phenomena,<sup>10</sup> remains to be fully established.

In (001) silicon quantum wells, the two valleys are isotropic, and similar experiments would enable direct comparisons between the roles of valley and spin in transport. By using a relatively recently discovered technique of exploiting a particular Si-SiO<sub>2</sub> interface,<sup>11</sup> we have been able to demonstrate that valley polarization also enhances resistivity in (001) silicon.<sup>12</sup> However, the out-of-plane electric field required to change valley polarization in these experiments also leads to a change in the bare disorder potential through the interface roughness, which also strongly affects resistivity, preventing direct comparisons from being made.

Here, we compare the magnitude of resistivity with and without spin and valley polarization under equivalent conditions of out-of-plane electric field and disorder. This is achieved by using both of the Si-SiO<sub>2</sub> interfaces of silicon-

on-insulator devices, one of which is a standard interface with negligible valley splitting, while the other is an interface with giant valley splitting.<sup>13</sup> A magnetic field up to 28 T is used to spin polarize electrons over a large density range. In combination, this enables us to complete a coarse but global description of the resistivity, demonstrating how electron density, spin-valley polarization, and disorder determine the resistivity in two dimensions. The data demonstrate that the temperature dependence can be changed in sign by each of these parameters and that magnetoresistivity and valley resistivity are, quantitatively, strikingly similar.

Our samples consist of a nominally 10-nm-thick layer of (001) silicon-on-insulator (SOI) patterned into Hall bars, the Ohmic contacts of which are degenerately doped with ion-implanted phosphorus. The active silicon layer is bound between a top-oxide layer formed by standard thermal oxidation and a lower buried oxide (BOX) layer formed by ion implantation of oxygen followed by high-temperature annealing (“SIMOX” process) [Fig. 1(a)]. The latter is known to give rise to a giant valley splitting as previously described in detail.<sup>11</sup> The electron density  $n$  is controlled by front and back gates with capacitances  $C_F = 463 \mu\text{Fm}^{-2}$  and  $C_B = 91.2 \mu\text{Fm}^{-2}$ , respectively, and is given by  $n = n_B + n_F$ , with  $n_F$  and  $n_B$  being electron densities contributed by the two respective gates. Valley splitting is controlled by tuning an effective out-of-plane electric field we quantify by a parameter  $\delta n = n_B - n_F$  which can be tuned independently of the total density  $n$ . The size of the valley splitting is approximated by a phenomenological formula:  $\Delta_V = \alpha \delta n$  when  $\delta n > 0 \text{ m}^{-2}$  where the valley factor  $\alpha$  for the Si-buried oxide interface in this study has a value of about  $0.49 \text{ meV}/10^{15} \text{ m}^{-2}$ . The valley splitting remains small when  $\delta n$  is negative [Fig. 1(b)]. Standard transport measurements were performed in a helium-4 variable temperature insert in a resistive magnet with field up to 28 T. The spin splitting is controlled by applying an in-plane magnetic field  $B_{\parallel}$  parallel to the current. Parallelism between the 2DES and the magnetic field is ensured by using a rotation stage and eliminating the Hall resistance.

In a single-particle picture in which each spin- and valley-split subband has density of states  $g = D_0 = m^*/2\pi\hbar^2$  [Fig. 1(c)] where  $m^*$  is the in-plane effective mass, a simple phase diagram can be constructed where the boundaries

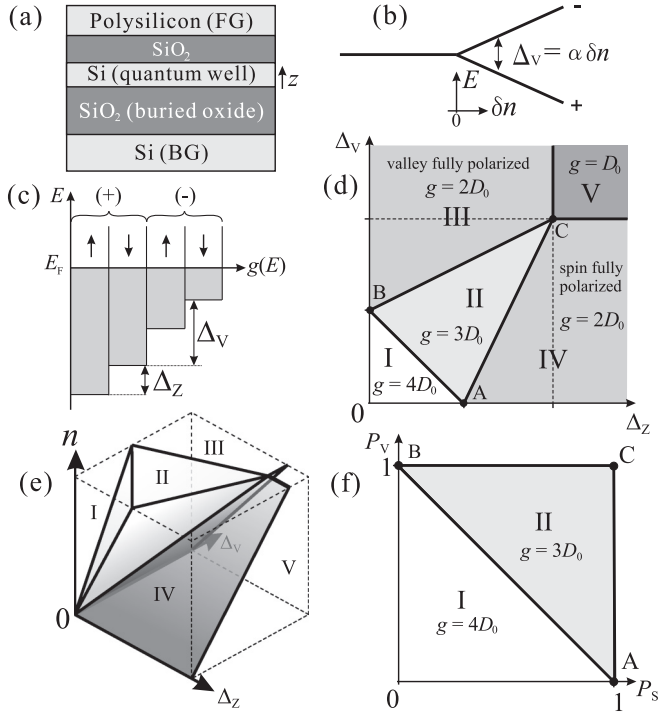


FIG. 1. (a) Schematic diagram of the sample. (b) Dependence of valley splitting  $\Delta_v$  on  $\delta n$ . (c) Spin- and valley-split subbands. (d) Single-particle phase diagram at constant density. (e) A three-dimensional visualization of (d) with  $n$  as a further parameter. (f) A phase diagram in terms of polarization.

represent the onset of occupation of a spin-valley-split subband at a constant sheet density  $n$  [Fig. 1(d)]. The boundaries are symmetric about the line  $\Delta_v = \Delta_z$  and each boundary scales with  $n$  linearly, collapsing to the origin at  $n = 0$  on the  $(\Delta_z, \Delta_v)$  plane [Fig. 1(e)]. The diagram can be simplified by defining spin and valley polarization:  $P_S = (n_\uparrow - n_\downarrow)/(n_\uparrow + n_\downarrow)$  and  $P_V = (n_+ - n_-)/(n_+ + n_-)$  where  $n_\uparrow$  and  $n_\downarrow$  are densities of electrons with up and down spin, respectively, while  $n_+$  and  $n_-$  are densities of electrons in two respective valleys [Fig. 1(f)].

Experimentally, the trajectory along the  $\Delta_z$  axis  $\{\Delta_v \sim 0$  [Fig. 1(d)] is achieved by keeping  $\delta n \leq 0 \text{ m}^{-2}$  while sweeping magnetic field. Thick black lines in Figs. 2(a)–2(f) show resistivity  $\rho_{xx}$  at  $\delta n = 0 \text{ m}^{-2}$  displaying the usual increase in resistivity with magnetic field as spins polarize, followed by saturation at full polarization.<sup>2,14–16</sup> With increased density  $n$ , the field at which saturation occurs ( $B_p$ ) increases as the Fermi energy increases.<sup>18</sup> On the other hand, the trajectory along  $\Delta_z \sim 0$  [Fig. 1(d)], along the  $\Delta_v$  axis, is achieved by sweeping  $\delta n$  (for  $\delta n > 0 \text{ m}^{-2}$ ) and the evolution of resistivity in these samples has already been described in detail.<sup>12</sup> Resistivity increases with  $\delta n$  in a similar manner as with spin polarization, followed by a shoulder feature rather than saturation, and continues to increase. In Fig. 2(d),  $\rho_{xx}$  is plotted at equal intervals of  $\delta n$ , and at zero magnetic field, there is a slight bunching of the traces near point B corresponding to the onset of full valley polarization. With increasing  $|\delta n|$ , there is an increase in the disorder potential due to interface roughness, as the out-of-plane wave function is pushed closer to the Si-SiO<sub>2</sub> interface and this in turn strongly enhances the resistivity,

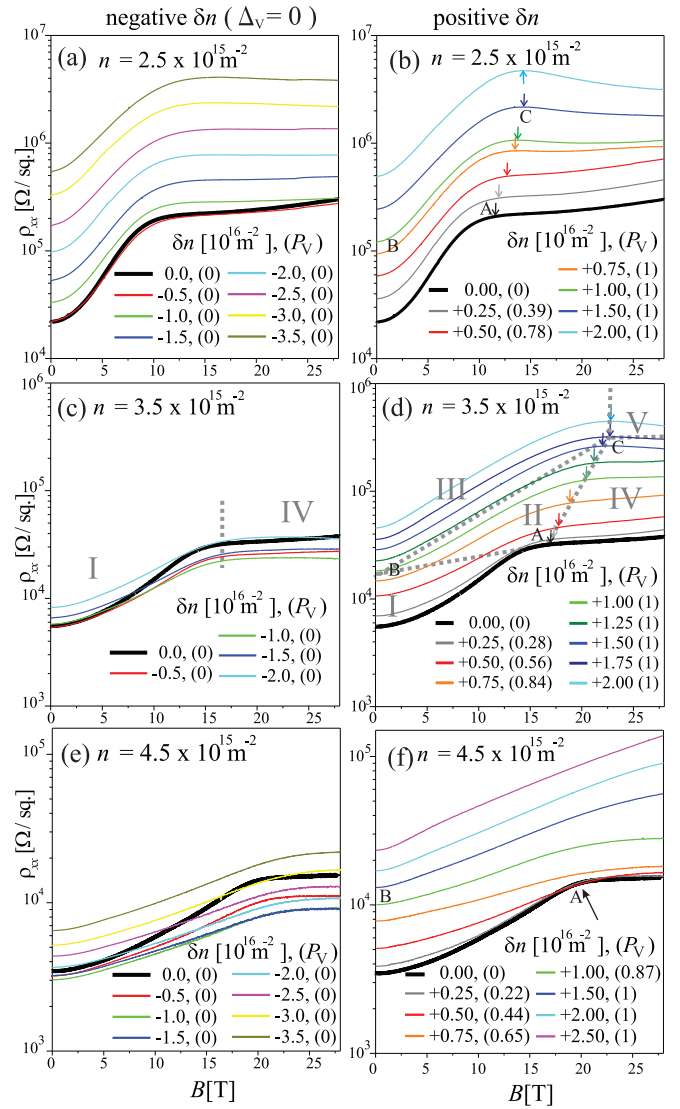


FIG. 2. (Color online) Magnetotransport at  $T = 1.4 \text{ K}$  as a function of  $\delta n$ . The left columns (a), (c), and (e) show data at negative  $\delta n$  ( $\Delta_v = 0$ ,  $P_V = 0$ ) while the right columns (b), (d), and (f) show data at positive  $\delta n$ . Each row corresponds to different density where (a) and (b),  $n = 2.5 \times 10^{15} \text{ m}^{-2}$ ; (c) and (d),  $n = 3.5 \times 10^{15} \text{ m}^{-2}$ ; and (e) and (f):  $n = 4.5 \times 10^{15} \text{ m}^{-2}$ . For each density (row), identical colors are used for identical values of  $|\delta n|$ . Small arrows are guides to the eye, marking the feature described in the body text.  $P_V$  in parentheses (Ref. 11) show values expected at zero magnetic field. Roman numerals in (c) and (d) show corresponding regions in Fig. 1(d) where the dotted line boundaries are straight line guides to the eye joining points A, B, and C.

and leads to an absence of saturation. This coupling of  $\delta n$  to disorder had previously prevented direct comparisons between valley resistance and magnetoresistance.

In order to assess the disorder potential in the absence of valley effects, we have recently performed experiments in a sample whose Si-SiO<sub>2</sub> interfaces were prepared by identical methods as those used in this study.<sup>13</sup> Holes, which do not possess the valley degree of freedom, show mobility which is almost symmetric in  $\delta n$ , in particular at large  $|\delta n|$  where

interface roughness is the dominant scattering mechanism. This indicates that the scale of interface roughness at the two interfaces are very alike and that the out-of-plane electric field dependence of the disorder potential are also very similar. We can therefore make a comparison of the resistivity with positive and negative  $\delta n$ , that is, with or without valley polarization, knowing that the bare disorder potential is similar for the same  $|\delta n|$ .

For negative  $\delta n$  at the lowest density [ $n = 2.5 \times 10^{15} \text{ m}^{-2}$  [Fig. 2(a)]], the resistivity increases with  $|\delta n|$  and the entire magnetoresistance trace shifts upwards on the logarithmic plot. The increase in zero-field resistivity indicates an increasingly large disorder potential, but the relative similarity of the curves shows that the factor by which the resistivity is enhanced by spin polarization is relatively constant and that there is not much qualitative change in the nature of the disorder.<sup>20,21</sup> At higher density [Fig. 2(c),  $n = 3.5 \times 10^{15} \text{ m}^{-2}$  and Fig. 2(e),  $n = 4.5 \times 10^{15} \text{ m}^{-2}$ ], the effects of negative  $\delta n$  are less dramatic.<sup>22</sup> This is presumably due to the ability of the electrons to screen the background disorder potential.

We now compare resistivity under valley polarization and spin degeneracy against spin polarization and valley degeneracy. These conditions correspond to  $(P_S, P_V) = (0, 1)$  [(1, 0)], which corresponds to point B (A) in Fig. 1(f) but a locus of points along the  $\Delta_V$  ( $\Delta_Z$ ) axis in region III (IV) in Fig. 1(d). Data are shown for two different densities and  $|\delta n|$  in Fig. 3. It can clearly be seen that there is considerable agreement between the data sets, providing strong evidence that valley and spin polarization play quantitatively equivalent roles in determining the value of the resistivity. The data do also show disagreement, especially at low density, in that data sets at  $(P_S, P_V) = (0, 1)$  and (1, 0) differ in temperature dependence, despite their similarity in the actual values of  $\rho_{xx}$ . For example, the low-density data in Fig. 3(b) show a crossover and, indeed, the discrepancy can be expected to grow at lower temperature. There will inevitably be differences in disorder at the two interfaces even if the hole mobilities are quantitatively very close,<sup>13</sup> and there is no direct correspondence between the value of magnetic field

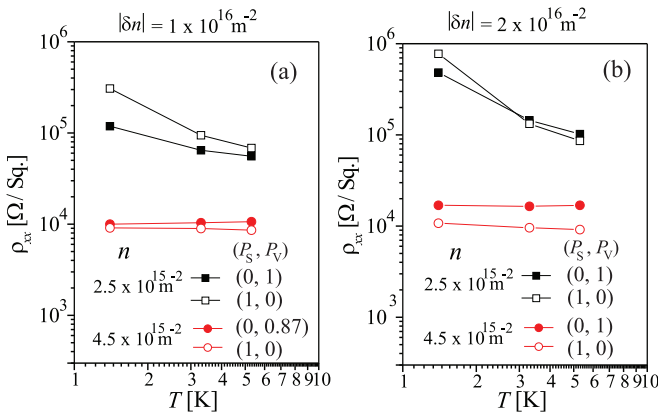


FIG. 3. (Color online) Comparison of the resistivity between spin-degenerate-valley-polarized and spin-polarized-valley-degenerate electrons at equal out-of-plane bias. (a)  $|\delta n| = 1 \times 10^{16} \text{ m}^{-2}$  and (b)  $|\delta n| = 2 \times 10^{16} \text{ m}^{-2}$ . Spin polarized data are taken at  $B = 28 \text{ T}$ .

used (28 T) and the “valley field” to expect exact agreements. However, we can also expect more physically fundamental differences such as differences between intervalley scattering and spin-flip scattering underlying the differences observed and makes an interesting prospect for future investigation.

We now address how the magnetoresistance changes with valley polarization at positive  $\delta n$ . Data are shown in Figs. 2(b), 2(d), and 2(f). At a density of  $n = 2.5 \times 10^{15} \text{ m}^{-2}$ , valley polarization occurs at around  $\delta n = 0.64 \times 10^{16} \text{ m}^{-2}$  at zero magnetic field.<sup>24</sup> In contrast to data at negative  $\delta n$ , positive  $\delta n$  clearly increases the field  $B_P$  at which the shoulder is observed. However, the single-particle picture predicts a doubling of this field [Fig. 1(d)], but this is clearly not what is observed, and only increases by a couple of Tesla, qualitatively consistent with previous measurements in AlAs.<sup>25,26</sup> The shift in  $B_P$  is clearer at higher density. At  $n = 3.5 \times 10^{15} \text{ m}^{-2}$  [Fig. 2(d)], saturation occurs at around  $B_P = 15.7 \text{ T}$  and this is seen to increase with increasing  $\delta n$  before saturating at around 22 T. Saturation of  $B_P$  with  $\delta n$  indicates the attainment of both spin and valley polarization [region V in Fig. 1(d)] and demonstrates that we can access all regions of the spin-valley phase diagram [Fig. 1(f)].<sup>27,28</sup> At a higher density of  $n = 4.5 \times 10^{15}$  [Fig. 2(f)],  $B_P$  increases from 20.8 T to beyond the field range of these experiments.

We now describe the global phenomenology of how the temperature dependence of resistivity changes with the key parameters [Figs. 4(a)–4(j)]. At zero magnetic field ( $B = 0 \text{ T}$ )

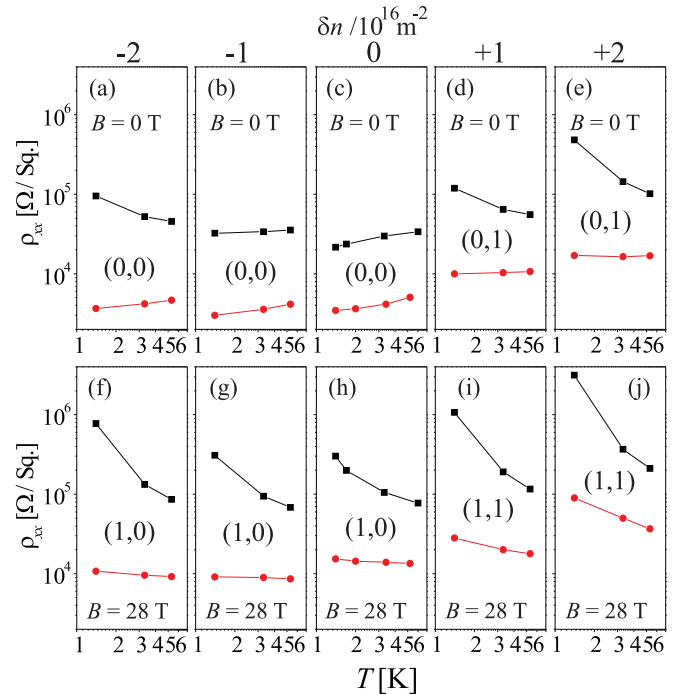


FIG. 4. (Color online) Temperature dependence of resistivity (squares:  $n = 2.5 \times 10^{15} \text{ m}^{-2}$ , circles:  $n = 4.5 \times 10^{15} \text{ m}^{-2}$ ). Data at  $B = 0 \text{ T}$  are shown in the top rows [(a)–(e)] while the lower rows [(f)–(j)] show data at  $B = 28 \text{ T}$ . Each column corresponds to a value of  $\delta n$ . Polarization  $(P_S, P_V)$  for  $n = 2.5 \times 10^{15} \text{ m}^{-2}$  is indicated in parentheses for each graph. Polarization at  $n = 4.5 \times 10^{15} \text{ m}^{-2}$  is the same except in (d) where  $P_V = 0.87$  and (i) and (j) where the degree of spin-valley polarization is substantial but not full.

and symmetry ( $\delta n = 0$ ) [Fig. 4(c)], both sets of data ( $n = 2.5 \times 10^{15} \text{ m}^{-2}$  and  $n = 4.5 \times 10^{15} \text{ m}^{-2}$ ) are on the metallic side of the so-called metal-insulator transition<sup>1-3</sup> (MIT)<sup>1-3</sup> and the resistivity decreases with decreasing temperature. With negative  $\delta n$ , disorder is increased and the critical density  $n_c$  of the MIT increases. The two-dimensional electron gas (2DEG) becomes insulating for  $n = 2.5 \times 10^{15} \text{ m}^{-2}$  representing a disorder-driven transition, while data at  $n = 4.5 \times 10^{15} \text{ m}^{-2}$  still display metallic behavior at  $\delta n = -2.0 \times 10^{16} \text{ m}^{-2}$  [Fig. 4(a)] and the absolute values are not very different to those at symmetry.

Under a strong magnetic field of 28 T, the 2DEG becomes insulating for both values of density, for all values of  $\delta n$ . This is a magnetic-field-induced transition to insulating behavior driven by spin polarization of the electrons. At low density, if the 2DEG shows insulating behavior [e.g., Fig. 4(a)], the insulating temperature dependence becomes even stronger [Fig. 4(f)] under spin polarization. In contrast, at higher density, the insulating temperature dependence is relatively mild. Similarly, with valley polarization at zero magnetic field [Figs. 4(d) and 4(e)], low-density data show a striking transition to insulating behavior while at high density ( $n = 4.5 \times 10^{15} \text{ m}^{-2}$ ) the system is very mildly metallic

at  $\delta n = 1 \times 10^{16} \text{ m}^{-2}$  [Fig. 4(d)] but almost temperature independent by  $\delta n = 2 \times 10^{16} \text{ m}^{-2}$  [Fig. 4(e)].

Finally, at large positive  $\delta n$  and high magnetic field, both spin and valley are fully polarized [Figs. 4(i) and 4(j)] for the lower density. Here, we find very strong insulating behavior which can be expected from the large values of resistivity, enhanced by both spin and valley polarization.

To summarize, we have presented a coarse but global phenomenology of how the resistivity depends on its key parameters: spin and valley polarization, density, and disorder. Similarities between the phenomenology when spin and valley polarization are exchanged provide strong evidence for quantitative equivalence in their roles played in the underlying physics.

K.T. is supported by the EPSRC of the UK (EP/I017860/1). Y.H. acknowledges support from JST-ERATO program. We are also supported by the European Commission from the 7th framework programme “Transnational Access,” Contract No. 228043-EuroMagNET II Integrated Activities Ref. GSC09-210. We are also grateful to D. Maude for support with experiments.

<sup>1</sup>B. Spivak, S. V. Kravchenko, S. A. Kivelson, and X. P. A. Gao, *Rev. Mod. Phys.* **82**, 1743 (2010).

<sup>2</sup>S. V. Kravchenko and M. P. Sarachik, *Rep. Prog. Phys.* **67**, 1 (2004).

<sup>3</sup>A. Prinz, V. M. Pudalov, G. Brunthaler, and G. Bauer, *Superlattices Microstruct.* **27**, 301 (2000).

<sup>4</sup>E. H. Hwang and S. Das Sarma, *Phys. Rev. B* **87**, 075306 (2013).

<sup>5</sup>Very recent examples include J. Isberg, M. Gabrysch, J. Jammersberg, S. Majdi, K. Kumar Kovi, and D. J. Twitchen, *Nat. Mater.* **12**, 760 (2013); C. H. Yang, A. Rossi, R. Ruskov, N. S. Lai, F. A. Mohiyaddin, S. Lee, C. Tahan, G. Klimeck, A. Morello, and A. S. Dzurak, *Nat. Commun.* **4**, 2069 (2013).

<sup>6</sup>M. Shayegan, E. P. De Poortere, O. Gunawan, Y. P. Shkolnikov, E. Tutuc, and K. Vakili, *Phys. Status Solidi B* **243**, 3629 (2006).

<sup>7</sup>M. Padmanabhan, T. Gokmen, and M. Shayegan, *Phys. Rev. Lett.* **104**, 016805 (2010); *Phys. Rev. B* **80**, 035423 (2009); **81**, 113301 (2010).

<sup>8</sup>O. Gunawan, Y. P. Shkolnikov, K. Vakili, T. Gokmen, E. P. De Poortere, and M. Shayegan, *Phys. Rev. Lett.* **97**, 186404 (2006).

<sup>9</sup>O. Gunawan, T. Gokmen, K. Vakili, M. Padmanabhan, E. P. De Poortere, and M. Shayegan, *Nat. Phys.* **3**, 388 (2007).

<sup>10</sup>For example, N. Tenen, A. Yu. Kuntsevich, V. M. Pudalov, and M. Reznikov, *Phys. Rev. Lett.* **109**, 226403 (2012).

<sup>11</sup>K. Takashina, Y. Ono, A. Fujiwara, Y. Takahashi, and Y. Hirayama, *Phys. Rev. Lett.* **96**, 236801 (2006).

<sup>12</sup>K. Takashina, Y. Niida, V. T. Renard, A. Fujiwara, T. Fujisawa, K. Muraki, and Y. Hirayama, *Phys. Rev. Lett.* **106**, 196403 (2011).

<sup>13</sup>Y. Niida, K. Takashina, Y. Ono, A. Fujiwara, and Y. Hirayama, *Appl. Phys. Lett.* **102**, 191603 (2013).

<sup>14</sup>T. Okamoto, K. Hosoya, S. Kawaji, and A. Yagi, *Phys. Rev. Lett.* **82**, 3875 (1999).

<sup>15</sup>V. T. Dolgoplov and A. Gold, *JETP Lett.* **71**, 27 (2000).

<sup>16</sup>At valley degeneracy and  $\delta n = 0$ , there is a relatively small but clearly visible positive magnetoresistance at a magnetic field much higher than  $B_p$  [Fig. 2(a)]. This can be attributed to orbital effects due to the upper confinement subband (Ref. 17). This is confirmed by its disappearance in measurements with negative  $\delta n$ . As  $|\delta n|$  increases, the difference in confinement energy between the ground subband and the first excited subband increases and effects of the first excited subband diminish.

<sup>17</sup>B. A. Piot, D. K. Maude, U. Gennser, A. Cavanna, and D. Mailly, *Phys. Rev. B* **80**, 115337 (2009).

<sup>18</sup>The values of  $B_p$  are, however, much lower than expected from the single-particle model. This is a well-established effect due to the many-body enhancement of the spin susceptibility, which in turn reduces  $B_p$  (Refs. 1 and 19).

<sup>19</sup>Y. Zhang and S. Das Sarma, *Phys. Rev. Lett.* **96**, 196602 (2006).

<sup>20</sup>T. M. Lu, L. Sun, D. C. Tsui, S. Lyon, W. Pan, M. Mühlberger, F. Schäffler, J. Liu, and Y. H. Xie, *Phys. Rev. B* **78**, 233309 (2008).

<sup>21</sup>The shoulder in resistivity which demarcates spin polarization does appear to shift slightly to higher field, but it is also broadened as one would expect from a stronger disorder potential.

<sup>22</sup>At small negative  $\delta n$ , the out-of-plane wave function still has a sufficiently large value at the Si-buried oxide interface to be affected by it. This has two consequences for the resistivity. First, the valley splitting itself can not be expected to go through zero as calculated by our phenomenological formula but to evolve continuously with a minimum at a small negative  $\delta n$  (Ref. 23). The polarization  $P_V$  would be a small fraction but may still affect resistivity. Second, we expect intervalley scattering to be enhanced by the Si-buried oxide interface, which is also known to reduce the 2DEG’s screening ability and enhance resistivity. The zero-field resistivity therefore falls before increasing with negative  $\delta n$ . This is more pronounced

for higher density where self-consistency effects tend to spread out the wave function.

<sup>23</sup>K. Takashina, A. Fujiwara, S. Horiguchi, Y. Takahashi, and Y. Hirayama, *Phys. Rev. B* **69**, 161304(R) (2004).

<sup>24</sup>This is a single-particle expectation extrapolated from behavior at higher densities (Refs. 11 and 12).

<sup>25</sup>T. Gokmen, M. Padmanabhan, and M. Shayegan, *Phys. Rev. Lett.* **101**, 146405 (2008).

<sup>26</sup>Y. P. Shkolnikov, K. Vakili, E. P. De Poortere, and M. Shayegan, *Phys. Rev. Lett.* **92**, 246804 (2004); T. Gokmen, M. Padmanabhan, and M. Shayegan, *Phys. Rev. B* **81**, 235305 (2010).

<sup>27</sup>It is interesting to note that for  $n = 4.5 \times 10^{15} \text{ m}^{-2}$  at  $\delta n \leq 0.5 \times 10^{16} \text{ m}^{-2}$  [Fig. 2(f)], even though the zero-field resistivity increases with  $\delta n$ , the magnetoresistance decreases and the resistivity at the shoulder at spin polarization shows a very slight decrease with  $\delta n$  [marked by the arrow in Fig. 2(f)]. Spin polarization at valley degeneracy corresponds to point A in Fig. 1(d) and increasing  $\delta n$  which increases valley splitting  $\Delta_V$  corresponds to moving vertically upwards into region II. We speculate that this negative valley resistance that we observe here is associated with valley polarization of localized states at the spin subband edge, analogous to the spin polarization of magnetic moments at the valley subband edge (Refs. 12, 29, and 30) at point B moving to the right also into region II in Fig. 1(d) (Ref. 31). In this case (point A), the negative

valley resistance would correspond to the suppression of a valley Kondo effect (Ref. 32) mediated by localized valley pseudospin moments.

<sup>28</sup>On the higher magnetic field side of the shoulder, the single-particle picture would predict a transition from region IV to region II with increased valley splitting, resulting in an *increase* in the density of states at the Fermi energy and a decrease in spin polarization. These would act to counter the effect of positive valley resistance from valley polarization. Nevertheless, we find the resistivity to increase smoothly and monotonically with  $\delta n$  excepting the direct vicinity of point A. We also note that we observe no strong feature in the magnetoresistance across the transition between regions I and II (Ref. 33).

<sup>29</sup>X. G. Feng, Dragana Popovic, and S. Washburn, *Phys. Rev. Lett.* **83**, 368 (1999).

<sup>30</sup>J. Kondo, *Prog. Theor. Phys.* **32**, 37 (1964).

<sup>31</sup>Negative magnetoresistance is not seen in Figs. 2(b), 2(d), and 2(f) due to the low density (Ref. 12).

<sup>32</sup>G. P. Lansbergen, G. C. Tettamanzi, J. Verduijn, N. Collaert, S. Biesemans, M. Blaauboer, and S. Rogge, *Nano Lett.* **10**, 455 (2010); S. Y. Shiau, S. Chutia, and R. Joynt, *Phys. Rev. B* **75**, 195345 (2007).

<sup>33</sup>This boundary can be observed at high density when the density is swept as previously described in Ref. 34.

<sup>34</sup>Y. Niida, K. Takashina, A. Fujiwara, T. Fujisawa, and Y. Hirayama, *Appl. Phys. Lett.* **94**, 142101 (2009).